JMEPEG (2012) 21:1107–1119
DOI: 10.1007/s11665-011-0006-1

1059-9495/$19.00

Fiber-Level Modeling of Dynamic Strength of Kevlar® KM2 Ballistic Fabric

M. Grujicic, A. Hariharan, B. Pandurangan, C.-F. Yen, B.A. Cheeseman, Y. Wang, Y. Miao, and J.Q. Zheng

(Submitted June 29, 2011)

In recent years, modeling of the high-performance ballistic fabric has gradually shifted from the continuum and yarn length scales to the sub-yarn length scale which enabled establishment of the relationships between the fabric penetration resistance and various fiber-level phenomena such as fiber-fiber friction, fiber twist, transverse properties of the fibers, and the stochastic nature of fiber strength. In general, these sub-yarn modeling schemes involve special numerical techniques (e.g., digital-element method) and customized computational codes. This status of the sub-yarn fabric-modeling methods and tools makes them not readily available to wider academic and industrial research communities. In the present work, an attempt is made to use conventional finite-element methods and tools in order to carry out sub-yarn numerical analysis of the penetration resistance of Kevlar® KM2 ballistic fabric. The goal was to demonstrate that results could be obtained which are comparable to their digital-element method = based counterparts. Specifically, a series of transient nonlinear dynamics finite-element analyses was carried out in order to investigate the role of the following two important sub-yarn phenomena on the penetration resistance of Kevlar® KM2 fabric: (a) fiber transverse properties including nonlinear elastic and plastic response and (b) fiber-fiber friction within the context of stochastically distributed fiber axial strength. It is generally found that the results obtained are consistent with their digital-element method-based counterparts.

Keywords ballistic performance, flexible armor, Kevlar® KM2 fibers and fabric, penetration resistance

1. Introduction

In order to respond to the new enemy threats and warfare tactics, military systems, in particular those supporting the U.S. ground forces, are being continuously transformed to become faster, more agile, and more mobile so that they can be quickly transported to operations conducted throughout the world. Consequently, an increased emphasis is being placed on the development of improved lightweight body-armor and lightweight vehicle-armor systems as well as on the development of new high-performance armor materials. High-performance fiber-based materials have been exploited for both body-armor (e.g., as soft, flexible fiber mats for personal-armor vests) and for the vehicle-armor systems (e.g., as reinforcements in rigid polymer matrix composites (PMCs) for lightweight vehicle-armor systems).

M. Grujicic, A. Hariharan, and **B. Pandurangan**, Department of Mechanical Engineering, Clemson University, 241 Engineering Innovation Building, Clemson, SC 29634-0921; **C.-F. Yen** and **B.A. Cheeseman**, Army Research Laboratory, Survivability Materials Branch, Aberdeen, Proving Ground, MD 21005-5069; **Y. Wang** and **Y. Miao**, Department of Mechanical and Nuclear Engineering, Kansas State University, Manhattan, KS 66506; and **J.Q. Zheng**, U.S. Army, PM-Soldier Equipment, Haymarket, VA 20169. Contact e-mail: gmica@clemson.edu.

Flexible lightweight materials have been used, throughout history, in body-armor systems to provide protection against specified threats, at reduced weight and without compromising person's mobility. Early materials used included leather, silk, metal chain mail, and metal plates. Replacement of metal with a nylon (*poly-amide*) fabric and an E-glass fiber/ethyl cellulose composite in body-armor systems can be linked to the Korean War (Ref 1). Although, primarily due to their low cost, nylon and E-glass fibers are still being used today, other nonnylon high-performance polymeric fibers (typically used in the form of woven fabrics) are now the standard in most fiber-reinforced body-armor applications. These high-performance polymeric fibers enabled the development of novel flexible-armor systems with exceptional protection against bullet penetration (Ref 2).

The defining characteristics of high-performance polymeric fibers used today are their superior strength, stiffness, and ballistic performance. Among these high-performance fibers the most notable are: (a) *poly-aramids* (e.g., Kevlar®, Twaron®, Technora®); (b) highly oriented *poly-ethylene* (e.g., Spectra®, Dyneema®); (c) *poly-benzobis-oxazole*, PBO (e.g., Zylon®); and (d) *poly-pyridobisimi-dazole*, PIPD (e.g., M5®). The present work is concerned with a particular grade of Kevlar® fibers, the Kevlar® KM2 fibers.

When tested in tension, the high-performance fibers mentioned above differ significantly from the nylon fibers, having very high absolute stiffness, extremely high density-normalized strength, and quite low ($<4\%$) strains-to-failure. These fibers essentially behave, in tension, as rate-independent linear elastic materials. When tested in transverse compression, however, these fibers are similar to nylon and can undergo large nonlinear elastic/plastic deformation without a significant loss in their tensile load carrying capacity. On the other hand, this behavior is quite different from that found in carbon or glass

Report Documentation Page

Form Approved
OMB No. 0704-0188

1. REPORT DATE	2. REPORT TYPE	3. DATES COVERED
JUL 2012		**00-00-2012 to 00-00-2012**

4. TITLE AND SUBTITLE	5a. CONTRACT NUMBER
Fiber-Level Modeling of Dynamic Strength of Kevlar KM2 Ballistic Fabric	5b. GRANT NUMBER
	5c. PROGRAM ELEMENT NUMBER
6. AUTHOR(S)	5d. PROJECT NUMBER
	5e. TASK NUMBER
	5f. WORK UNIT NUMBER
7. PERFORMING ORGANIZATION NAME(S) AND ADDRESS(ES) **Clemson University,Department of Mechanical Engineering,241 Engineering Innovation Building,Clemson,SC,29634**	8. PERFORMING ORGANIZATION REPORT NUMBER
9. SPONSORING/MONITORING AGENCY NAME(S) AND ADDRESS(ES)	10. SPONSOR/MONITOR'S ACRONYM(S)
	11. SPONSOR/MONITOR'S REPORT NUMBER(S)

12. DISTRIBUTION/AVAILABILITY STATEMENT
Approved for public release; distribution unlimited

13. SUPPLEMENTARY NOTES

14. ABSTRACT

15. SUBJECT TERMS

16. SECURITY CLASSIFICATION OF:			17. LIMITATION OF ABSTRACT	18. NUMBER OF PAGES	19a. NAME OF RESPONSIBLE PERSON
a. REPORT **unclassified**	b. ABSTRACT **unclassified**	c. THIS PAGE **unclassified**	**Same as Report (SAR)**	**13**	

fibers, which tend to shatter under transverse compression loading conditions (Ref 3).

While the attention above was focused on fibers and the associated materials, it should be recognized that flexible-armor structures are made of fabric/textiles containing these fibers. The fabric itself possesses a hierarchical structure, i.e., fibers are arranged into bundles called yarns and yarns are assembled into fabric in specific patterns through weaving or braiding processes. It is important to note that fabric ballistic-penetration resistance is influenced not only by fiber physical properties, such as strength, ductility, elastic modulus, mass-density, viscosity and thermal properties, but also by fabric architecture in its as-fabricated state.

Although attempts were made as early as the 1960s to guide the development of new flexible-armor systems using computer-aided-engineering and modeling/simulation approaches, the design and development of textile armor systems remains primarily governed by experiments and experience. While numerical models typically have not been used to guide the design/development of the new flexible-armor systems, they have been frequently employed to quantify the effect of specific fiber/yarn/fabric parameters on the ballistic-penetration resistance of the armor (Ref 4, 5). Furthermore, it should be noted that, while, it is well established that the fabric performance is highly affected by the fabric-manufacturing process and the as-fabricated architecture, most of the flexible-armor ballistic-penetration numerical models either fail to include or include incompletely/incorrectly the effect of fabric microstructural parameters such as yarn denier, end count, yarn structures, filament spatial paths and fiber-to-fiber interactions. Consequently, a quantitative relation among material properties, manufacturing process, fabric micro-geometry, and ballistic performance could not be established by these models.

This deficiency of the flexible-armor numerical models has been recently addressed in a series of papers by Wang and co-workers (Ref 6-12) who proposed a new method, the so-called ''Digital-Element Method.'' In this method, a yarn is represented as an assembly of colinear regularly spaced discrete fibers. Each fiber, in turn, is modeled as a chain composed of short truss elements with the adjacent trusses being connected via friction-less spherical joints. To model the contact between adjacent fibers, contact elements are introduced adaptively, i.e., at the places at which the distance between two fibers is smaller than fiber diameter. The main objective of the present work is to demonstrate that the ''Digital-Element Method'' can be cast as a conventional finite-element analysis problem and that it can be implemented into a commercial finite-element code.

It is important to note that the level of details of the fabric architecture used in the numerical model influences the resolution and the accuracy/fidelity of the numerical results obtained (Ref 13-16). For example, if a fabric is considered as a continuum, details of yarn-to-yarn interaction and projectile-to-yarn interaction cannot be modeled. Consequently, the effect of fabric weave pattern on ballistic resistance cannot be analyzed. On the other hand, if the fabric is represented as an assembly of inter-woven yarns but the yarns are represented as a continuum, details of fiber-to-fiber interaction and projectile-to-fiber interaction cannot be modeled. Consequently, the effect of yarn microstructure on the ballistic resistance cannot be analyzed.

A review of the public-domain literature carried out as part of the present work revealed that the numerical models of the flexible-armor systems can be broadly divided into two groups: (a) those in which the fabric is modeled as a continuum and (b) those in which the fabric architecture is accounted for explicitly but the yarns are treated as a continuum.

While there are a relatively large number of continuum-fabric numerical models developed since the 1970s, the most representative of these appear to be (i) a homogeneous and isotropic plate model which deforms into a straight-sided conical shell when impacted by a projectile (Ref 17, 18); (ii) a two-dimensional isotropic membrane model (Ref 19); (iii) an anisotropic membrane model (Ref 20); (iv) a model based on the use of a system of linear springs to represent continuum behavior (Ref 21); and (v) a visco-elastic continuum model with rate-dependent failure (Ref 22). While all of these models claim to be in good agreement with the associated experimental results, they are, as mentioned above, unable to account for yarn-to-yarn and projectile-to-yarn interactions, which have been shown to influence the flexible-armor ballistic performance (Ref 23, 24).

In the most recent renditions of the continuum-fabric numerical models, the concept of the unit-cell is used in order to derive the equivalent (smeared-out) continuum-level (membrane/shell) material models of flexible armor from the knowledge of the meso-scale fiber and yarn properties, fabric architecture and inter-yarn and inter-ply frictional characteristics. The term ''meso-scale'' is used to denote yarn-level millimeter length scale details of the fabric microstructure/architecture. In other words, finer-scale molecular-level and fiber-level material details are not considered explicitly and instead only their lumped contributions are taken into account. The ''unit-cell'' term is used to denote the basic structural unit in a woven single-ply fabric so that a fabric patch can be considered as an in-plane assembly of such units. Among the most notable studies based on these analyses are those carried out by Kawabata et al. (Ref 25-27) who introduced simple analytical models to capture the uniaxial, biaxial, and shear behavior of fabrics. Furthermore, Ivanov and Tabiei (Ref 28) proposed a micro-mechanical material model for a woven fabric (in which a visco-elastic constitutive model was used to represent the mechanical behavior of the yarns) for the use in nonlinear finite-element impact simulations. In deriving the material model, Ivanov and Tabiei (Ref 28) considered the motion of the yarn-crossover point and developed a procedure for determining the equilibrium position of this point under the applied unit-cell strains. Recently, King et al. (Ref 29) proposed a new approach for deriving the continuum-level material model for fabrics based on the properties of the yarns and the weave architecture which involves the use of an energy minimization technique to establish the relationship between the configurations of the fabric structure to the microscopic deformation of fabric components. Similar unit-cell based continuum-level membrane/shell material models have been developed by Boisse et al. (Ref 30) and Peng and Cao (Ref 31). Also, Shahkarami and Vaziri (Ref 32) proposed a similar but simpler model to that introduced by King et al. (Ref 29) and provided a detailed account of its incorporation into a material-model subroutine which can be readily coupled with commercial dynamic-explicit finite-element codes.

Among the flexible-armor numerical models falling into the second category the most representative appear to be: (i) the model developed by Roylance and co-workers who simplified a two-dimensional woven fabric as a two-dimensional network of pin-jointed short filaments. In the model, the filament longitudinal stiffness and strength are set equal to their fiber/yarn counterparts. The model was subsequently extended to include

the contribution of other material/contact/microstructural parameters such as yarn slippage (Ref 33), projectile geometries and fabric-clamping conditions (Ref 34), nonlinear visco-elastic effects (Ref 35), multiple-ply fabric architecture (Ref 36), yarn crimp (Ref 37), and slip at yarn-crossover points (Ref 38). Despite all these improvements, the pin-jointed filament-network model fails to capture the contribution of fabric topology and yarn micro-geometry to the flexible-armor ballistic-penetration resistance; (ii) the model developed by Shockey et al. (Ref 39) which represents the first finite-element model in which each individual yarn was discretized using solid/continuum elements. The model was applied to the case of a turbine blade impacting a containment shroud. This model was extended to the case of fabric impact by spherical and right-circular cylindrical fragment simulating projectiles (FSPs) by Duan et al. (Ref 40, 41). Additional expansions of the Shockey model were also made in order to account for the effects of multi-ply ballistic fabric (Ref 42, 43) and different weaving patterns (Ref 44); and (iii) the model of Zohdi and Powell (Ref 45), in which the fabric is represented as an assembly of cross-woven yarns, yarns are modeled as bundles of collinear fibers while fibers are treated as continuum elements.

The main objective of the present work is to extend the use of conventional transient nonlinear dynamics finite-element simulations to the sub-yarn length scale and to compare the results with both the computational ones obtained by Wang and co-workers (Ref 11, 12) (using the digital-element method), and with the corresponding experimental results reported in Ref 11, 12.

The organization of the article is as follows: A brief overview of the Kevlar® KM2 fiber, yarn, and fabric properties is provided in section 2. The problem of normal impact of a spherical projectile onto a square patch of Kevlar® KM2 fabric clamped along its edges and the computational procedure employed are described in section 3. The role of fiber transverse properties in the behavior of ballistic fabric during impact by a projectile is analyzed in section 4. The effect of friction and the stochastic nature of the Kevlar® KM2 fiber strength are discussed in section 5. A general discussion of the results obtained is presented in section 6. The main summary points and conclusions resulting from the present work are listed in section 7.

2. Kevlar® KM2 Fiber, Yarn, and Fabric Properties

2.1 Fiber Properties

Experimental investigation of Chen et al. (Ref 46, 47), clearly established that, in the longitudinal direction, Kevlar® KM2 fiber behaves as a rate-independent inelastic material with an average longitudinal Young's Modulus of 84.62 ± 4.18 GPa with 95% confidence. As far as the longitudinal strength, σ, is concerned, it is found to be a stochastic property (due to inevitable presence of various microstructural defects/imperfections within the fibers) and to be implicitly given by a bi-modal Weibull-type failure-distribution function, $F(\sigma)$, in the form (Ref 48):

$$F(\sigma) = 1 - \exp\left[-\frac{L}{L_0}\sum_{i=1}^{n}\left(\frac{\sigma}{\sigma_{0i}}\right)^{m_i}\right] \quad \text{(Eq 1)}$$

where $n = 2$ (due to the bi-modal nature of the distribution function), $L_0 = 0.025$ m (the fiber reference gage length), L (the fiber actual gage length), $\sigma_{01} = 3.323$ GPa and $\sigma_{02} = 3.7004$ GPa (the two Weibull scale parameters) and $m_1 = 18.0023$ and $m_2 = 24.8803$ (the two Weibull shape parameters). The bi-modal nature of the Kevlar® KM2 fiber strength is related to the distinct defect/flaw potency distributions in the core and in the skin regions of this class of fibers.

While in the transverse direction, Kevlar® KM2 fibers show nonlinear and inelastic behavior, following the work of Wang and co-workers (Ref 11), the constitutive response of the fibers in the transverse direction is modeled at three different levels of physical accuracy/fidelity: (a) at the highest level of approximation, the response is treated as being linear elastic with the associated transverse modulus of 1.34 ± 0.35 GPa (with 95% confidence); (b) the response is considered to be nonlinear elastic with the loading/unloading nominal stress $\bar{\sigma}$ versus nominal strain $\bar{\varepsilon}$, relation given as:

$$\bar{\sigma} = 0.006e9 + 0.5296e9\bar{\varepsilon} - 1.2208e9\bar{\varepsilon}^2 + 6.9417e9\bar{\varepsilon}^3 \quad \text{(Eq 2)}$$

where the nominal stress is defined as a ratio of the contact force and the product of the fiber diameter and the fiber length, while the nominal strain was defined as the ratio of the fiber diameter change and the fiber diameter; and (c) at the highest level of fidelity, the transverse response is considered as being elastic/plastic with Eq 2 defining the strain hardening yielding behavior of the fiber during loading (involving plastic deformation) while elastic unloading/reloading is defined as:

$$K = 0.0646e9 + 7.0632e9\bar{\varepsilon}_{\max} + 18.666e9\bar{\varepsilon}_{\max}^2 \quad \text{(Eq 3)}$$

where $\bar{\varepsilon}_{\max}$ is the maximum transverse normal strain experienced by the local material point of the fiber.

It should be noted that since fiber transverse stiffness provides little contribution to either fabric or yarn transverse stiffness, one cannot generally determine fiber transverse properties by testing yarns or the fabric. Instead, testing must be done using individual fibers (Ref 46, 47).

2.2 Yarn Properties

It should be noted that yarns are represented in the present work as a bundle of collinear discrete fibers. Hence, yarn properties are not defined as input parameters to the numerical model but rather could be assessed through the appropriate postprocessing schemes. Nevertheless, it should be recognized that the yarn longitudinal properties are directly controlled by the fiber longitudinal properties. For example, the longitudinal stiffness modulus of the yarns is defined as a product of the fiber longitudinal stiffness modulus and a $(1 - F(\sigma))$ factor in order to account for the effect of potential fiber failure.

As far as the yarn transverse properties are concerned, they are mainly controlled by yarn microstructure, fiber/fiber friction, and yarn tension.

2.3 Fabric Properties

As in the case of the yarns, fabric properties are not defined as input parameters to the numerical mode but rather could be assessed through the appropriate postprocessing schemes. In general, both the longitudinal and transverse properties of the fabric depend on the fabric areal density, yarn count per fabric unit length, longitudinal properties of the fibers and yarns,

fabric architecture/weave pattern, fiber/fiber friction, and yarn tension. The Kevlar® KM2 fabric analyzed in the present work has an areal density of 180 g/m^2 and 13.4 yarns per centimeter. The fabric contains a plain-woven architecture which is obtained by "snaking" through orthogonally oriented warp and weft yarns.

3. Problem Definition and Computational Procedure

In this section, a brief description is provided of the projectile/fabric-impact problem analyzed in the present work and of the computational procedure employed.

3.1 Problem Definition

The basic problem analyzed in the present work involves the impact of a 8-mm diameter steel spherical projectile, mass = 2.1 g, with a 33 × 33 mm^2 patch of a Kevlar® KM2 fabric clamped along all its four edges. Only the normal impact (i.e., zero obliquity angle) case is considered. The projectile incident velocity is varied in 35-210 m/s range.

3.2 Geometrical Model

The initial geometrical model for the projectile/fabric assembly is shown in Fig. 1(a). A close-up of the fabric is displayed in Fig. 1(b) in order to reveal the plain-weave fabric architecture and the (7-fiber) sub-yarn microstructure.

The fabric architecture and its areal density were defined in section 2.3. The fabric test patch included 42 (warp) yarns and 42 (weft) yarns. Each yarn is discretized into discrete circular-cross-section fibers bundled into a regular (identical) hexagonal close-packed configuration. Various yarn discretizations were initially considered, Fig. 2(a)-(f), in the initial portion of the work in order to identify the one which provides the best trade-off between the physical accuracy and computational cost. For each of the configurations considered fiber diameter was calculated in such a way that the correct fabric areal density is obtained. Fibers are treated as discrete circular-section solid entities. Yarns are treated as bundles of linearly collinear transversely interacting fibers, while the fabric is treated as a plain-woven structure consisting of nearly orthogonal warp and weft yarns.

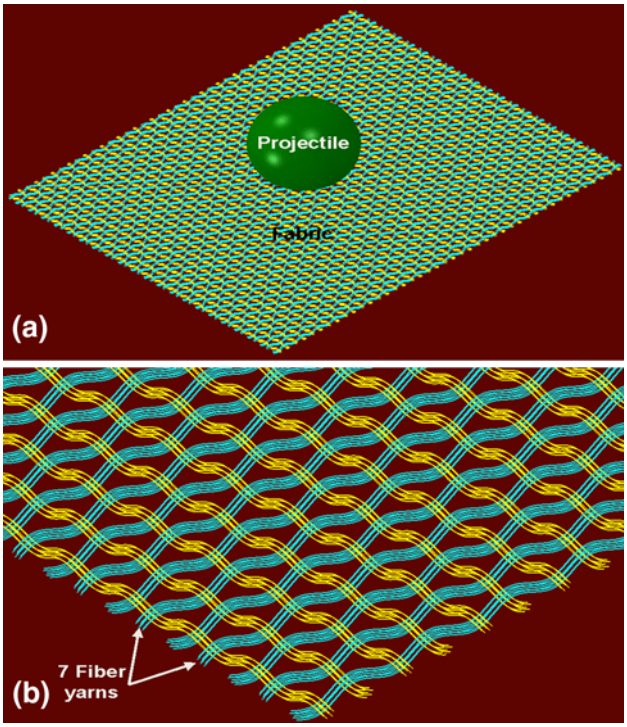

Fig. 1 (a) A geometrical model for the projectile/fabric interaction problem analyzed in the present work and (b) a close-up of the fabric region showing sub-yarn microstructure and the yarn-weave pattern

3.3 Finite-Element Model

Within the finite-element model each fiber is discretized into a number of three-dimensional beam elements with the beam length chosen to match the fiber diameter. The material properties for Kevlar® KM2 fibers were defined in section 2.1. It should be noted, as will be discussed in more detail below, that the longitudinal properties of the fibers are specified within the material definition while the transverse properties are specified as a part of the fiber/fiber contact definition.

The spherical projectile is discretized using continuum first-order tetrahedron elements with an edge length comparable to the fiber beam-element length. Due to the fact that the steel projectile used in the experimental studies relevant to the present work (Ref 11), did not suffer any permanent deformation during impact testing, the projectile material (steel) is treated as an isotropic linear elastic material with a Young's Modulus of 210 GPa and a Poisson's ratio of 0.3.

At the beginning of the analysis, the following initial conditions are specified: (a) the projectile is assigned a preselected negative value of the velocity z-component (the mid-plane of the fabric is placed on the xy-plane associated with $z = 0$, while initially the projectile center of gravity is placed at $x = y = 0$ and $z >$ projectile radius); and (b) the fabric is assumed to be stress-free, deformation-free and at rest.

As mentioned earlier, during the simulation the fabric is fully clamped along all its four edges (the boundary conditions).

The response of the fibers in the transverse directions, due to fiber/fiber and fiber/projectile normal interactions, is modeled using a contact algorithm implemented within the *VUINTER* user subroutine of the commercial finite-element package ABAQUS/Explicit (Ref 49). Within this subroutine, the fiber transverse constitutive relations defined in Eq 2 and 3 are implemented. Within the same subroutine, tangential fiber/fiber and fiber/projectile interactions are modeled using a simple Coulomb-type friction law within which the transmission of shear stresses across the contact interfaces is defined in terms of static and kinetic friction coefficients and an upper-bound shear stress limit (a maximum value of shear stress which can be transmitted before the contacting surfaces begin to slide).

Within a portion of the present work, fiber-fracture strength is treated as a stochastic quantity. In this case, a Monte Carlo procedure is employed within which a random number in a range (0,1) is drawn (for each fiber element) from the uniform distribution and assigned to the failure probability of the element in question. Then, the Eq 1 is solved for the unknown fracture strength of the material residing within this element. Within the ABAQUS/Explicit (Ref 49) computational environment, the

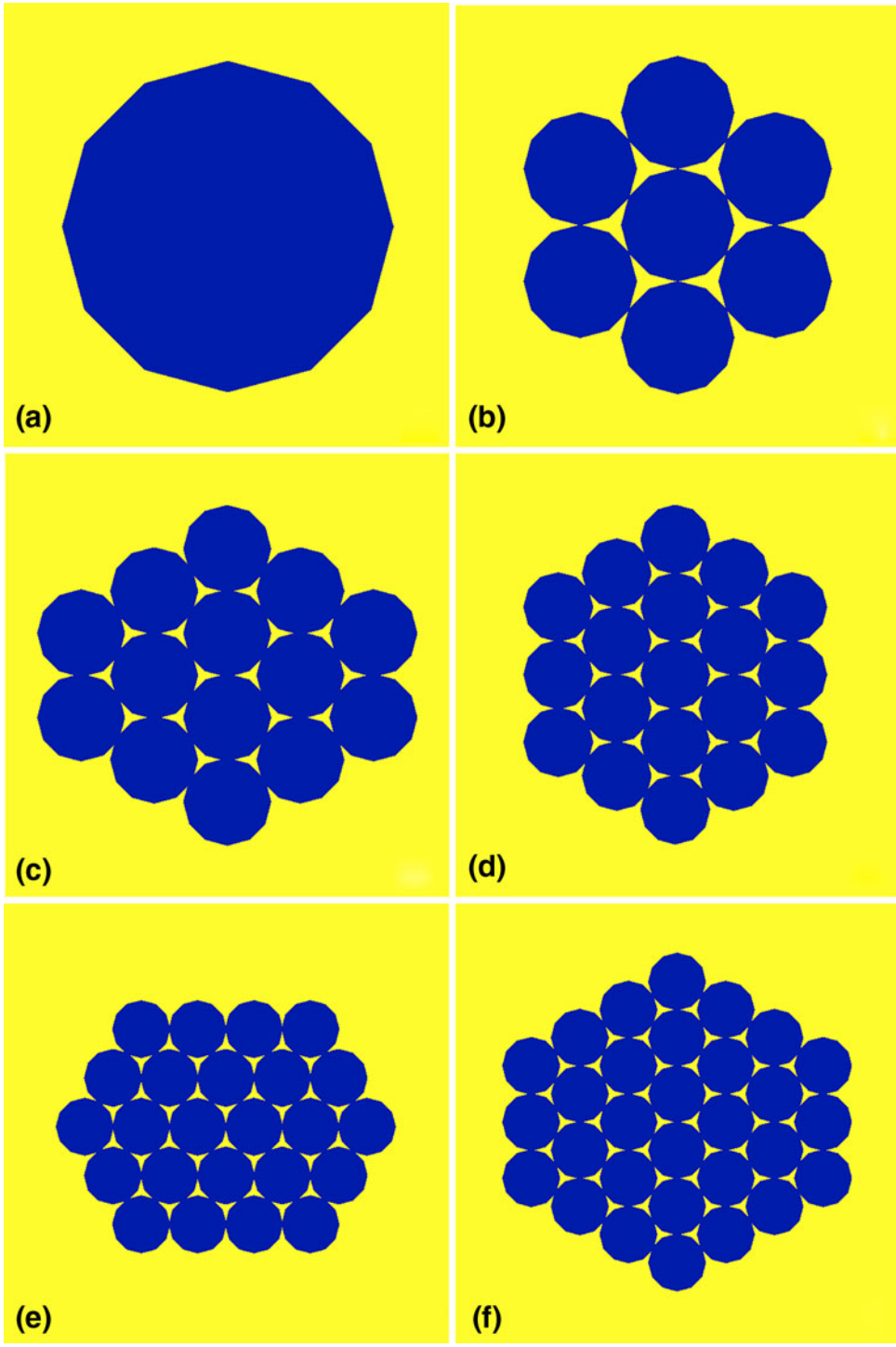

Fig. 2 Various yarn microstructures considered in the present work: (a) single-fiber yarn, (b) 7-fiber yarn, (c) 14-fiber yarn, (d) 19-fiber yarn, (e) 24-fiber yarn, and (f) 30-fiber yarn

most efficient way to implement the stochastically distributed fiber-fracture strength is through the use of a user material subroutine VUMAT. Within this subroutine, material strength associated with a given beam element/integration-point is treated as a material-state variable. This variable retains its initially assigned value until the onset of fiber failure (i.e., until the axial stress becomes equal to the material strength) and then decreases monotonically to zero (in a manner consistent with the preassigned value of the material toughness).

3.4 Computational Procedure

All the calculations carried out in the present work were done using ABAQUS/Explicit (Ref 49) within which the problem at hand defined in terms of a set of mass, momentum, and energy conservation differential equations along with the material constitutive relations and contact, initial and boundary conditions is solved using a finite-element approach. A typical 210 μs projectile/fabric computational analysis based on

14-fiber yarns required 3.5 h of (wall-clock) time on a 12 core, 3.0 GHz machine with 16 GB of memory.

It should be noted that an attempt was made in the present work to include the effect of the weaving process on to the architecture/microstructure of the fabric used in the present impact simulations. Specifically, a separate computational analysis was conducted first in order to include the potential effect of the weaving process on the yarn cross section. Within this analysis, fiber ends were subjected to axial outward loads. The loads were first linearly ramped to a maximum value and then linearly ramped back to zero. The maximum value of the loads was selected in such a way that the corresponding yarn force is 1 N (a typical value of the yarn stretching loads accompanying fabric weaving). Due to the creation of relatively high contact forces between the crossing fibers, the yarn cross-sectional area in the cross-over region was found to change from the circular ones, displayed in Fig. 2(a)-(f), to the oval ones (with the major axis running horizontally). To include first-order effects of the weaving process on the fabric architecture, all the subsequent fabric penetration-resistance analyses were done using the fabric with the oval-shaped yarns.

4. The Effect of Fiber Transverse properties

When a projectile strikes the flexible-armor/fabric, it applies transverse loading either directly or indirectly (through fiber-to-fiber contacts) to the fibers and yarns constituting the flexible armor. As clearly established in the recent work of Wang and co-workers (Ref 11), fiber transverse properties play an important role in the ballistic performance of flexible armor. Hence, one of the main objectives of the present work is to extend the use of conventional transient nonlinear dynamics finite-element simulations to the sub-yarn length scale and to

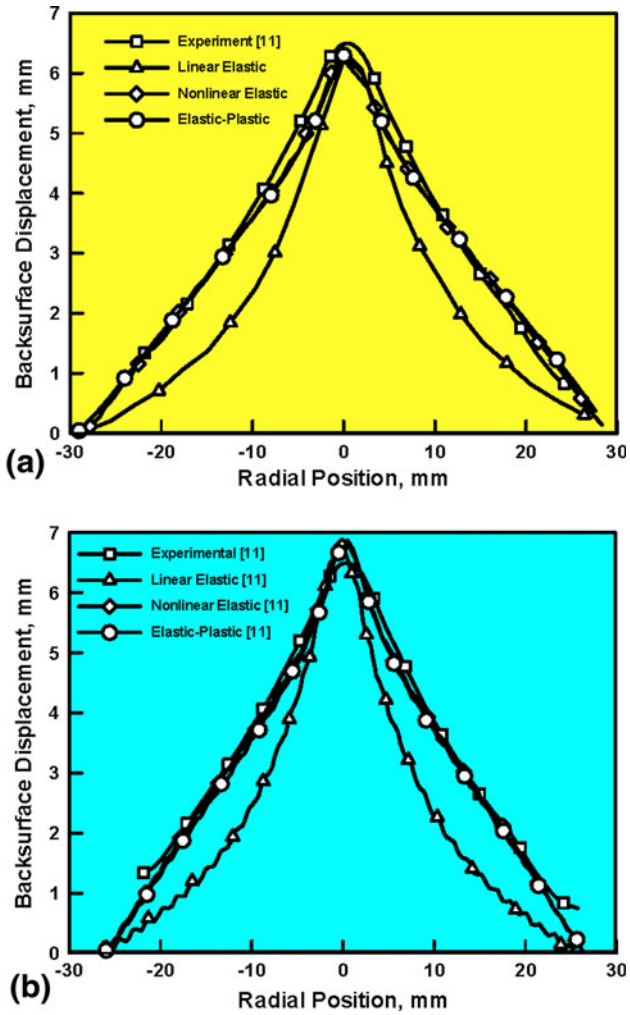

Fig. 3 Variation of the fabric back-surface displacement with the radial distance from the fabric center for the case of 2.1 g steel spherical projectile impacting the Kevlar KM2 fabric at an initial velocity of 63 m/s: (a) present computational results; and (b) computational results from Ref 11. In both (a) and (b), the experimental results from Ref 11 are shown

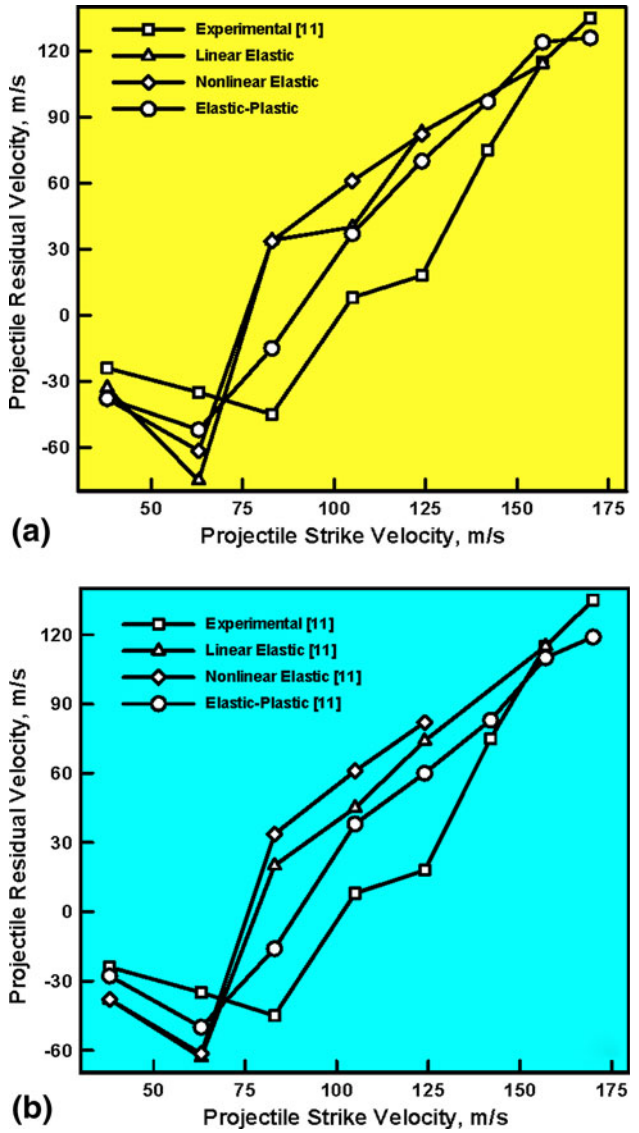

Fig. 4 Variation of the projectile residual/rebound velocity with the projectile initial velocity for the case of 2.1 g steel spherical projectile impacting the Kevlar KM2 fabric: (a) present computational results and (b) computational results from Ref 11. In both (a) and (b), the experimental results from Ref 11 are shown. Rebound velocities are assigned negative values

compare the computational results pertaining to the effect of fiber transverse properties on the penetration resistance of the Kevlar® KM2 fabric with the ones obtained by Wang and co-workers (Ref 11) (using the digital-element method and the experimental measurements).

4.1 Observation/Findings of Wang and Co-workers (Ref 11)

Wang and co-workers (Ref 11) clearly established that fiber transverse properties play an important role in the ballistic performance of flexible armor affecting the magnitude of the projectile residual velocity (the velocity of the projectile after it has defeated the flexible armor or has been defeated by the armor), fabric transverse-displacement profile, fabric's ability to deform and absorb/dissipate the projectile's kinetic energy, the stress magnitude/distribution within the fibers and the overall armor strength. When a projectile strikes flexible armor, there are two general outcomes: (a) the projectile is defeated by the flexible armor and it rebounds and (b) the projectile penetrates the flexible armor while retaining a portion of its initial velocity (typically referred to as the residual velocity).

In the case of projectile defeat one can generally identify four distinct phases of the projectile/fabric interaction: (i) on the initial contact, both the projectile and the ''influenced region'' of the fabric move in the projectile-traveling direction with a progressively lower velocity; (ii) the projectile is brought to rest; (iii) the projectile and the fabric begin to rebound at a progressively higher velocity; and (iv) the projectile separates from the fabric and continues to move in the reverse direction with a constant velocity. Since neither projectile nor the fabric suffers typically any significant damage in this process, it is the temporal evolution of the projectile and fabric velocities and the fabric transverse-displacement profile which are generally used to validate a flexible-armor numerical model in this regime of the projectile/target interaction. In the case of the flexible-armor defeat by the projectile, on the other hand, it is the projectile residual velocity and the temporal evolution and spatial distribution of the fabric damage/failure which is used in the numerical-model validation.

The work of Wang and co-workers (Ref 11) clearly established that if Kevlar® KM2 fibers are treated as rate-independent linear elastic materials in the transverse direction, the digital element-based numerical model for the flexible armor shows significant disagreement with respect to the corresponding experimental findings in the following four areas:

(a) The computed projectile rebound velocity is nearly equal (in magnitude) to while the corresponding experimental velocity is significantly smaller than the projectile incident velocity. This finding indicates that the ability of the fabric to absorb and dissipate the kinetic energy of the projectile is considerably under-predicted;
(b) The ballistic-penetration resistance of the flexible armor as quantified by the v_{50} (the velocity at which a projectile has a 50% chance of penetrating the armor) is underestimated typically by 20-25% signaling that the attendant energy absorption/dissipation processes are not properly accounted for;

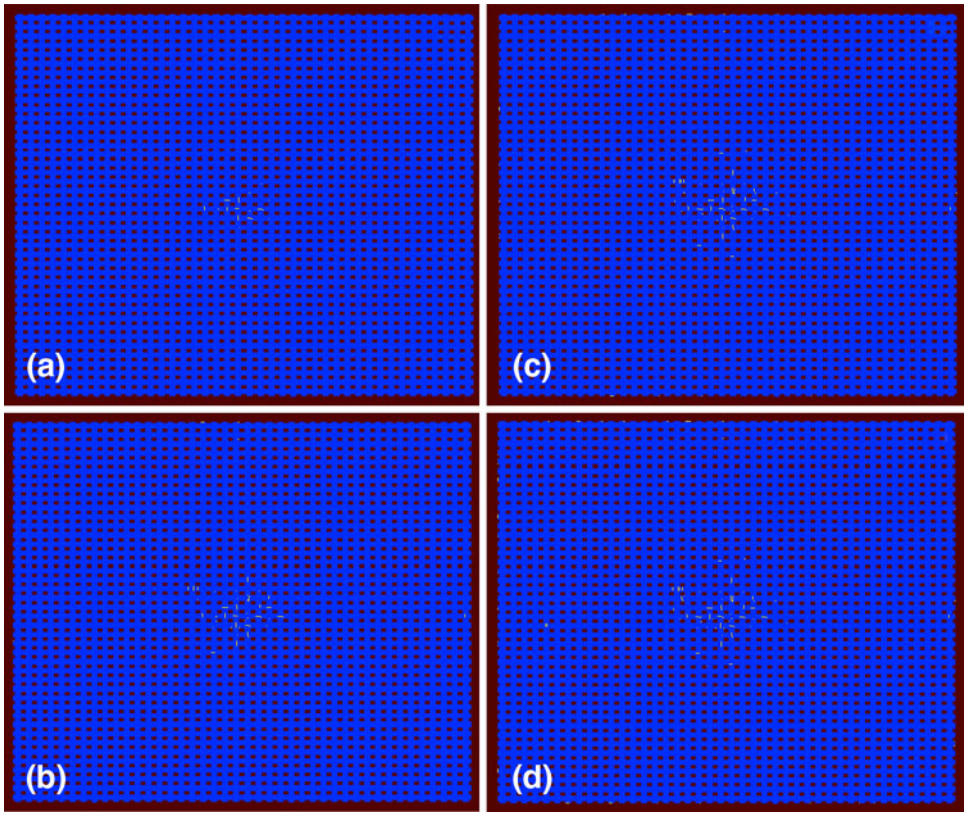

Fig. 5 Spatial distribution of the fabric damage during impact by a 2.1 g steel spherical projectile traveling at an initial velocity of 63 m/s for the case of a deterministic fiber-fracture strength (=3.4 GPa) at postimpact times of (a) 75, (b) 120, (c) 165, and (d) 210 μs. Damaged elements (white) and undamaged elements (black) are shown using the undeformed fabric mesh and the projectile is not shown

(c) In the cases when the projectile initial velocity exceeds the v_{50}, the projectile residual velocity is generally over-predicted by 20-25%, again suggesting that the numerical model at hand fails to properly account for the attendant energy-dissipation processes; and
(d) The computed and the experimentally measured spatial distribution and the temporal evolution of the fabric transverse displacement are very different.

Wang and co-workers (Ref 11) further showed that if Kevlar® KM2 fibers are treated as rate-independent nonlinear elastic materials in the transverse direction, the digital element-based numerical model for the flexible armor still shows significant (although somewhat lesser with respect to the transverse linear elastic fiber case) disagreement with respect to the corresponding experimental findings in the areas of the projectile rebound velocity, v_{50} and the projectile residual velocity. However, the computed and the experimentally measured spatial distribution and the temporal evolution of the fabric transverse displacement are quite similar in this case.

When the Kevlar® KM2 fibers are treated as rate-independent elastic-plastic materials in the transverse direction, Wang and co-workers (Ref 11) showed that the digital-element method predicts the projectile's rebound, v_{50}, residual velocities as well as the flexible armor transverse-displacement spatial distribution and temporal evolution in a reasonably good agreement with their experimental counterparts.

Finally, Wang and co-workers (Ref 11) showed that fiber transverse properties control the maximum axial stress within the fibers and, in turn, the fabric strength. That is, an increase in the fiber's ability to undergo transverse compressive deformation lowers the extent of fiber longitudinal extension (and thus longitudinal peak stress) during the projectile/fabric-impact process. This, in turn, reduces the probability for fiber failure and increases the overall flexible-armor ballistic strength. The ability of the fiber to undergo transverse strain is facilitated by at least two phenomena: (a) a low magnitude of the fiber transverse modulus (e.g., in Kevlar® KM2 fibers the transverse modulus is only about 1/60 of the longitudinal modulus); and (b) a relatively low transverse yield strength (150 MPa), respectively, in the case of Kevlar® KM2 fiber.

4.2 Present Work Results and Their Comparison with Those of Wang and Co-workers (Ref 11)

The results obtained in the present work pertaining to the radial distribution of the fabric back face nodal displacements in the projectile-propagation (z) direction for the case of projectile initial velocity of 63 m/s and the postimpact time of 0.174 ms are displayed in Fig. 3(a). Three sets of the computational results are displayed in this figure, one for each of the three (linear elastic, nonlinear elastic, and elastic-plastic) fiber transverse-response conditions. For comparison, the experimental results reported in Ref 11 are also depicted in this figure.

For further comparison, the computational results of Wang and co-workers (Ref 11) based on the use of the digital-element method along with the associated experimental results (Ref 11) are displayed in Fig. 3(b).

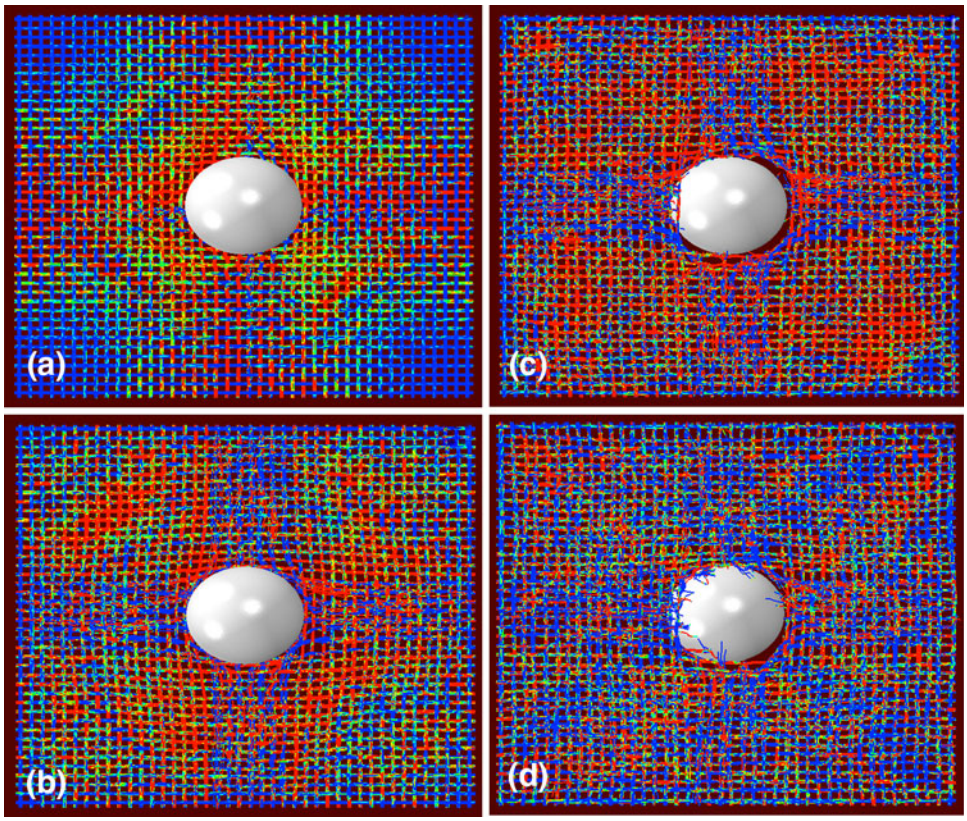

Fig. 6 Spatial distribution of fiber axial stress during impact by a 2.1 g steel spherical projectile traveling at an initial velocity of 63 m/s for the case of a deterministic fiber-fracture strength (=3.4 GPa) at postimpact times of (a) 75, (b) 120, (c) 165, and (d) 210 μs

A simple comparison of the Fig. 3(a) and (b) reveals that the corresponding computational results obtained using the two computational schemes is mutually in reasonable agreement and that the elastic-plastic analysis (in both cases) yields the best overall agreement with the experimental data.

The results obtained in the present work pertaining to the effect of the projectile initial velocity on its residual/rebound velocity are displayed in Fig. 4(a). Three sets of computational results are displayed in this figure, one for each of the three (linear elastic, nonlinear elastic, and elastic-plastic) fiber transverse-response conditions. For comparison, the experimental results reported in Ref 11 are also depicted in this figure. It should be noted that when the projectile is defeated and rebounds, its rebounding velocity is shown as a residual velocity with a negative value.

For further comparison, the computational results of Wang and co-workers (Ref 11) based on the use of the digital-element method along with the associated experimental results (Ref 11) are displayed in Fig. 4(b).

Simple comparison of the Fig. 4(a) and (b) shows that the two computational schemes yield the results which are comparable under the given (linear elastic, nonlinear elastic, and elastic-plastic) fiber transverse-response conditions. In addition, in both cases, the elastic-plastic analysis has been found to yield the best overall agreement with the experimental data.

5. The Effect of Fiber-Fiber Friction and the Stochastic Nature of the Fiber Strength

As clearly established in the recent work of Wang and co-workers (Ref 12), fiber-fiber and fiber-projectile friction has a major effect on the penetration resistance of high-performance ballistic fabric and also affects the role of the stochastic nature of the fiber strength onto the fabric ballistic performance. Hence, the other main objective of the present work is to compare the finite-element-based computational results (pertaining to the effect of friction and stochastic character of the fiber strength on the fabric penetration resistance) with the ones obtained by Wang and co-workers (Ref 12) (using the digital-element method and the experimental measurements).

5.1 Observation/Findings of Wang and Co-workers (Ref 12)

In regard to the phenomenon of fiber failure, in general, and the roles of fiber-fiber friction and the stochastic nature of fiber

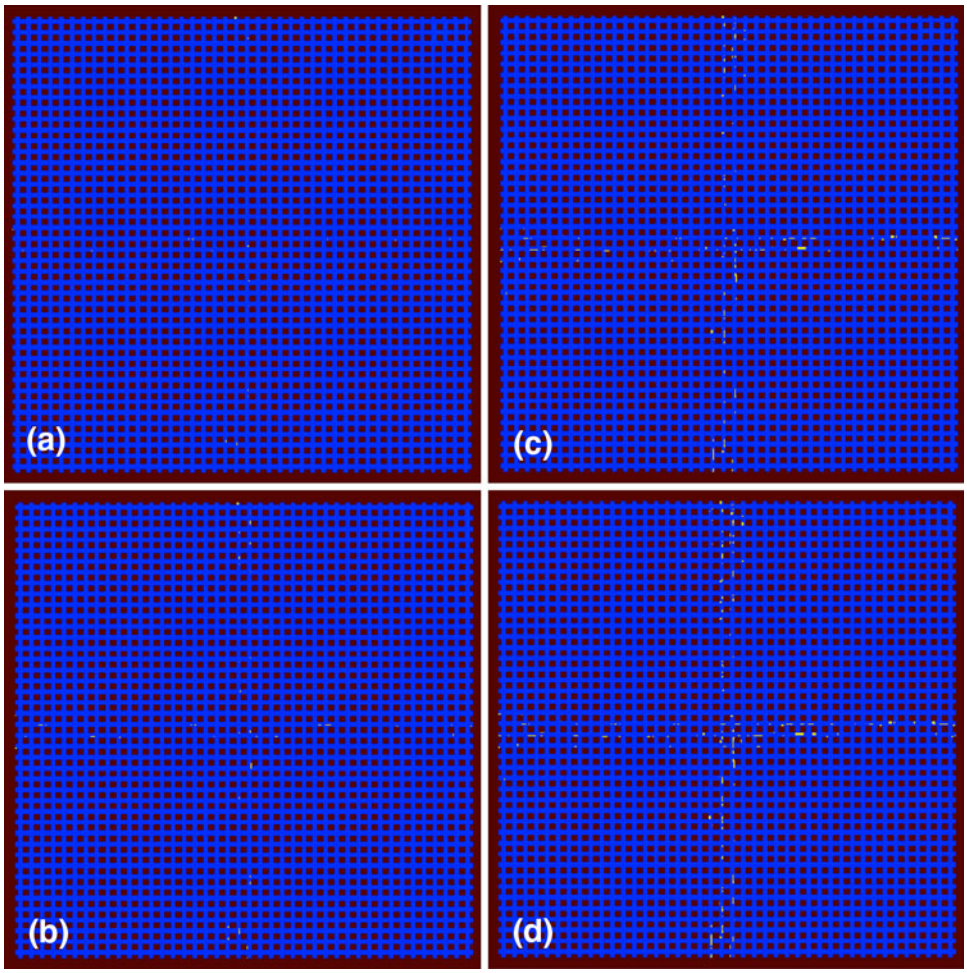

Fig. 7 Spatial distribution of the fabric damage during impact by a 2.1 g steel spherical projectile traveling at an initial velocity of 63 m/s for the case of stochastic fiber-fracture strength at postimpact times of (a) 140, (b) 150, (c) 170, and (d) 180 μs

strength, in particular, during impact of a projectile onto the fabric, the work of Wang and co-workers (Ref 12) established the following:

(a) Failure of a (stretched) fiber is followed by a fairly complex stress-redistribution/unloading process which can be divided into three well-defined stages: (i) the propagation of the release waves from the fractured ends of the two fiber fragments toward the clamped end of these fragments. The swept region of the fiber fragments is fully relieved of the prior tensile longitudinal stress; (ii) the release waves become arrested at one of the yarn/yarn-crossover points producing locally a high level of tensile stress; and (iii) transmitted release waves are emitted from the high-stress region toward the clamped end of the fiber fragments reducing the extent of stress concentration and increasing the average level of tension in the loaded portion of the fiber fragments;
(b) the distance travelled by the release waves, before their arrest, scales inversely with the magnitude of the fiber-fiber friction coefficient;
(c) if, and when, the enhanced average level of tension defined in (a), (iii) exceeds the fiber local failure strength, the fiber fracture as well as the aforementioned stress-redistribution processes reoccur;
(d) in the case of the reoccurring fracture of the fibers, the average fragment length scales inversely with the magnitude of the fiber-fiber friction coefficient;
(e) the deterministic versus stochastic nature of the fiber strength affects both the magnitude of the fabric ballistic-penetration resistance, the morphology of the fabric-fracture process as well as the role of the fiber-fiber friction coefficient;
(f) when fiber strength is treated as a deterministic quantity, fabric failure appears to be a local phenomenon and occurs in the highest-stress region (the region which is in direct contact with the projectile tip). In this case, a lower magnitude of the friction coefficient gives rise to a longer length of the tension-free region of the fractured fiber(s). This enables the projectile to more readily push aside the fractured fibers and to defeat the fabric. However, due to the local nature of the fiber failure process, the effect of the magnitude of fiber-fiber friction coefficient on the fabric ballistic strength is relatively weak;
(g) when fiber strength is treated as a stochastic quantity, fabric failure appears to be a nonlocal phenomenon and generally occurs not in the high-stress region but rather in the regions associated with the most potent microstructural imperfections/flaws in the fibers. Typically, these regions are located outside the impacted fabric region and the associated release waves mentioned above can cause a spread of the fiber fracture into the fabric-impact region. In other words, the fabric-fracture process becomes a nonlocal phenomenon in this case. Since the average fiber fragment length is controlled by the fiber-fiber friction coefficient, the magnitude of the friction coefficient tends to play a more significant role than in the deterministic case;
(h) when the projectile incident velocity substantially exceeds v_{50}, the deterministic versus stochastic nature of

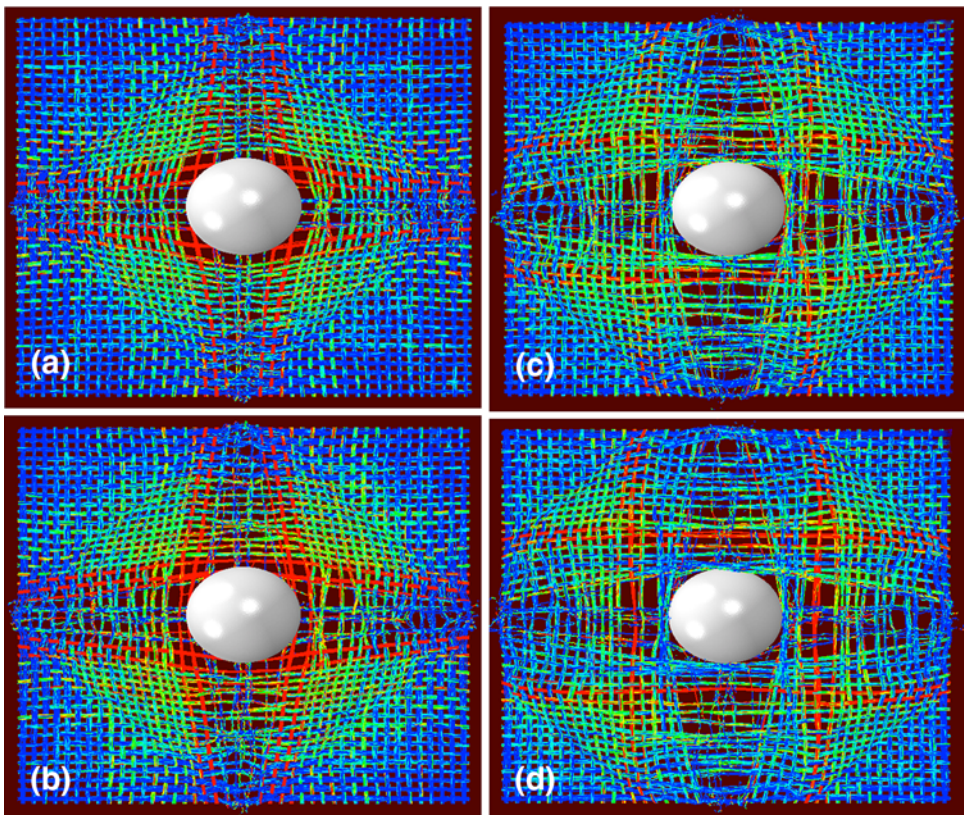

Fig. 8 Spatial distribution of fiber axial stress during impact by a 2.1 g steel spherical projectile traveling at an initial velocity of 63 m/s for the case of stochastic fracture strength at postimpact times of (a) 140, (b) 150, (c) 170, and (d) 180 μs

the fiber strength has little effect on the projectile residual velocity or on the projectile/fabric interaction process in general. The fabric failure in this case is a local phenomenon occurring in the fabric-impacted region. That is, although in the stochastic case the fabric initial failure can occur outside the impacted region, insufficient time is available for this fracture to spread into the impact region before full penetration of the fabric takes place.

5.2 Present Work Results and Their Comparison with Those of Wang and Co-workers (Ref 12)

Since all of the computational and experimental results reported in the work of Wang and co-workers (Ref 12) were obtained using fabric test patches with an edge length of 101.6 mm or larger while the present computational analysis (due to the limitations on the computing resources) involved fabric test patches with an edge length of 33 mm, a direct quantitative comparison of the two sets of results could not be carried out. Instead, the present computational effort was aimed at validating the previously overviewed general findings obtained in the work of Wang and co-workers (Ref 12).

Typical results pertaining to the spatial distribution of the fabric damage during impact by a 2.1 g steel spherical projectile traveling at an initial velocity of 63 m/s for the case of a deterministic fiber-fracture strength (=3.4 GPa) at four different postimpact times (75, 120, 165, and 210 μs) is displayed in Fig. 5(a)-(d). It should be noted that for improved clarity, the results in this figure are displayed using the undeformed fabric mesh and the projectile is not shown. The damaged/broken fiber elements are depicted using white color, while the undamaged elements are shown in black. Examination of the results displayed in Fig. 5(a)-(d) shows that the fabric damage, in the deterministic fiber-strength case, is mainly localized in the region underneath the projectile. This finding is fully consistent with the ones reported by Wang and co-workers (Ref 12).

Typical results pertaining to the spatial distribution of fiber axial stress under the impact conditions identical to the ones stated in conjunction with Fig. 5(a)-(d) are shown in Fig. 6(a)-(d). In this case, the fabric deformed mesh and the projectiles are shown. Examination of the results displayed in Fig. 6(a)-(d) confirms the general digital element-based computational and experimental findings of Wang and co-workers (Ref 12) that fabric penetration is a local process. In other words, penetration of the fabric is mainly controlled by the creation and evolution of damage in the fabric region which is beneath and, hence, directly impacted by the projectile.

Typical results pertaining to the spatial distribution of the fabric damage during impact by a 2.1 g steel spherical projectile traveling at an initial velocity of 63 m/s for the case of stochastic fiber-fracture strength at four different postimpact times (140, 150, 170, and 180 μs) is displayed in Fig. 7(a)-(d). It should be noted that for improved clarity, the results in this figure are displayed using the undeformed fabric mesh and the projectile is not shown. The damaged/broken fiber elements are depicted using white color, while the undamaged elements are shown in black. Examination of the results displayed in Fig. 7(a)-(d) shows that the fabric damage, in the stochastic fiber failure-strength case, initiates in a region not directly impacted by the projectile and then advances toward the impacted region. This finding is fully consistent with the ones reported by Wang and co-workers (Ref 12).

Typical results pertaining to the spatial distribution of fiber axial stress under the impact conditions identical to the ones stated in conjunction with Fig. 7(a)-(d) are shown in Fig. 8(a)-(d). In this case, the fabric deformed mesh and the projectiles are shown. Examination of the results displayed in Fig. 8(a)-(d) confirms the general digital element-based computational and experimental findings of Wang and co-workers (Ref 12) that fabric penetration is a nonlocal process. In other words, fiber damage is typically initiated in the fabric region which is not directly in contact with the projectile but contains high-potency flaws/defects. The resulting redistribution of the stress within the fibers and the formation of high-stress regions leads to spreading of damage toward the region impacted by the projectile. Thus, fabric penetration is no longer a local phenomenon and is highly affected by the distributed nature of fabric failure strength.

The effect of the magnitude of the fiber-fiber friction coefficient on the penetration frequency of the fabric by the projectile for the case of deterministic fiber-fracture strength is displayed in Fig. 9(a). Clearly, due to the deterministic nature

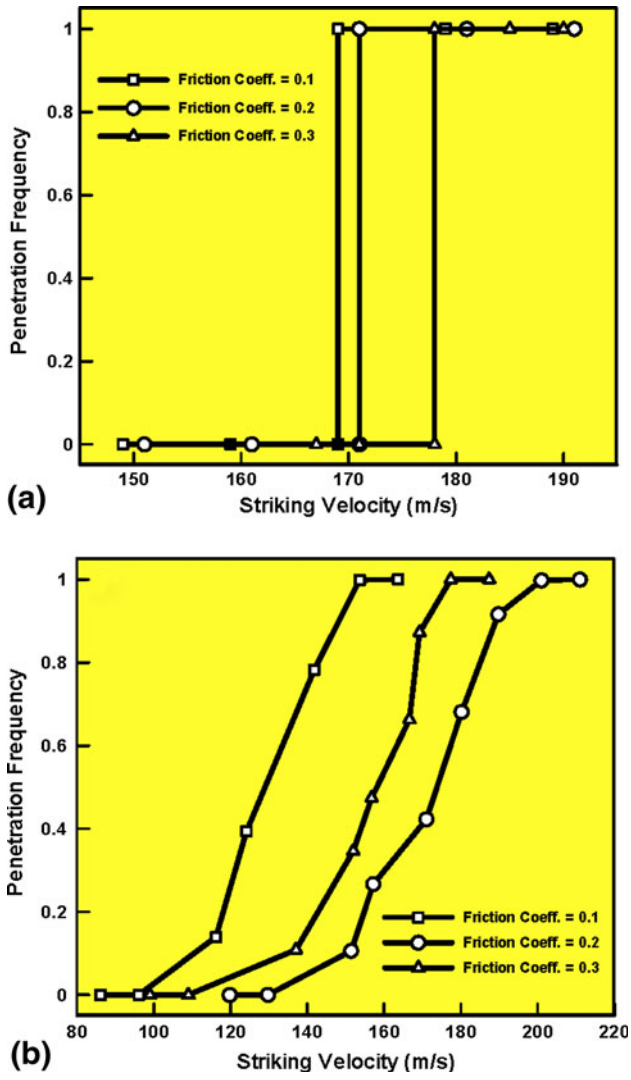

Fig. 9 Variation of penetration frequency of the fabric by the projectile with the magnitude of the fiber-fiber friction coefficient for the case of (a) deterministic fiber-fracture strength and (b) stochastic fiber-fracture strength

of the fiber strength, the results obtained under nominally identical conditions are fully repeatable. Hence, the curves shown in Fig. 9(a) are of a step-function type. The results displayed in this figure confirm the general digital element-based computational and experimental findings of Wang and co-workers (Ref 12) that: (a) a higher value of the fiber-fiber friction coefficient increases the fabric's penetration resistance (as quantified by the projectile velocity at which the penetration frequency changes from zero to one) and (b) the effect of friction coefficient on the fabric penetration resistance is relatively weak.

The effect of the magnitude of the fiber-fiber friction coefficient on the penetration frequency of the fabric by the projectile for the case of stochastically distributed fiber-fracture strength is displayed in Fig. 9(b). Due to the stochastic nature of the fiber strength, the penetration frequency versus projectile strike velocity curves are no longer step-function like. Instead, there is a range of projectile velocities between the maximum velocity at which no penetration occurs and a minimum velocity at which penetration always occurs. The results displayed in this figure confirm the general digital element-based computational and experimental findings of Wang and co-workers (Ref 12) that: (a) there is an optimal value of the fiber-fiber friction coefficient which is associated with the maximum value of the fabric penetration resistance and (b) the effect of fiber-fiber friction coefficient on fabric penetration resistance is substantially stronger in the case of the stochastic nature of the fiber strength than in the deterministic case.

6. A Brief Discussion

It should be recalled that the main objective of the present work is to extend the use of conventional transient nonlinear dynamics finite-element simulations to the sub-yarn length scale and to compare the results with both the computational ones obtained by Wang and co-workers (Ref 11, 12) (using the digital-element method), and with the corresponding experimental results reported in Ref 11, 12. The description of the finite-element analysis presented in section 3 showed how the sub-yarn fabric modeling and simulations which are commonly done using the digital-element method and in-house developed codes could be carried out using a commercial finite-element package. The results presented and analyzed in sections 4 and 5 demonstrated that the present approach is fully consistent with the digital-element computational approach and that the results are in agreement with their experimental counterparts (Ref 11, 12). It should be noted, however, that there are additional computational and experimental results reported in Ref 11, 12, these results were obtained using fabric test patches whose size is too big to be modeled using the computational resources available in the present work. Nevertheless, the level of agreement between the results obtained in the present work and the ones reported in Ref 11, 12 is such that there is no reason to doubt that the present approach could adequately predict the ballistic performance of the larger fabric test patches.

7. Summary and Conclusions

Based on the material-model development procedure used and the results of the subsequent computational analyses, the following main summary remarks and conclusions can be drawn:

1. A sub-yarn (i.e., a fiber length scale) material model has been developed for Kevlar® KM2 ballistic fabric within a conventional finite-element framework.
2. The model is used to determine the penetration resistance of this fabric and its overall deflection, deformation and damage response during impact by a spherical projectile.
3. To validate the present computational procedure, the results obtained are compared with their computational (digital-element method based) and experimental counterparts.
4. Particular attention has been given to identifying and quantifying the effects of fiber transverse properties, fiber-fiber friction and the stochastic nature of fiber-fracture strength on the overall ballistic performance of the high-performance flexible armor fabric.
5. Overall, the results obtained in the present work are found to be in reasonable agreement with their computational (digital-element method based) and their experimental counterparts.

Acknowledgments

The material presented in this article is based on work supported by the Army Research Office (ARO) research contract entitled "Multi-length Scale Material Model Development for Armor-grade Composites," Contract Number W911NF-09-1-0513, and the Army Research Laboratory (ARL) research contract entitled "Computational Analysis and Modeling of Various Phenomena Accompanying Detonation Explosives Shallow-Buried in Soil" Contract Number W911NF-06-2-0042.

References

1. R.E. Wittman and R.F. Rolsten, Armor of Men and Aircraft, *12th National SAMPE Symposium, SAMPE*, 1967
2. The Interceptor System, US Marine Corps, http://www.marines.mil/marinelink/image1.nsf/lookup/200532317129?opendocument
3. M. Grujicic, B. Pandurangan, D.C. Angstadt, K.L. Koudela, and B.A. Cheeseman, Ballistic-Performance Optimization of a Hybrid Carbon-Nanotube/E-glass Reinforced Poly-Vinyl-Ester-Epoxy-Matrix Composite Armor, *J. Mater. Sci.*, 2007, **42**, p 5347–5359
4. M. Grujicic, W.C. Bell, L.L. Thompson, K.L. Koudela, and B.A. Cheeseman, Ballistic-Protection Performance of Carbon-Nanotube Doped Poly-Vinyl-Ester-Epoxy Composite Armor Reinforced with E-glass Fiber Mats, *Mater. Sci. Eng. A*, 2008, **479**, p 10–22
5. M. Grujicic, W.C. Bell, S.B. Biggers, K.L. Koudela, and B.A. Cheeseman, Enhancement of the Ballistic-Protection Performance of E-glass Reinforced Poly-Vinyl-Ester-Epoxy Composite Armor via the Use of a Carbon-Nanotube Forest-Mat Strike Face, *Mater. Des. Appl.*, 2008, **222**, p 15–28
6. Y. Wang and X. Sun, Determining the Geometry of Textile Performs using Finite Element Analysis, *Proceedings of the American Society for Composites, 15th ASC Technical Conference on Composite Materials*, Vol 9, September 24-27, College Station, TX, 2000, p 25–27
7. X. Sun and Y. Wang, Geometry of 3-D Braiding Rectangular Perform with Axial Yarns, *Proceedings of the 46th International SAMPE Symposium*, Vol 46, Long Beach Convention Center, CA, 2001, p 2455–2464
8. Y. Wang and X. Sun, Digital Element Simulation of Textile Processes, *J. Compos. Sci. Technol.*, 2001, **63**, p 311–319
9. G. Zhou, X. Sun, and Y. Wang, Multi-Chain Digital Analysis in Textile Mechanics, *J. Compos. Sci. Technol.*, 2003, **64**, p 239–244

10. Y. Miao, E. Zhou, Y. Wang, and B. Cheeseman, Mechanics of Textile Composites: Micro-Geometry, *J. Compos. Sci. Technol.*, 2008, **68**(7-8), p 1671–1678
11. Y. Miao, Y. Wang, J. Yu, C.-F. Yen, D. Swenson, and B.A. Cheeseman, Effects of Fiber Transverse Properties on Fabric Penetration Resistance, *Int. J. Impact Eng.*, 2011 (submitted)
12. Y. Wang, Y. Miao, C.-F. Yen, B.A. Cheeseman, and J.Q. Zheng, Effects of Fiber Friction Coefficient on Fabric Penetration Resistance, *Int. J. Impact Eng.*, 2011 (submitted)
13. M. Grujicic, G. Arakere, T. He, M. Gogulapati, and B.A. Cheeseman, A Numerical Investigation of the Influence of Yarn-Level Finite-Element Model on Energy Absorption by a Flexible-Fabric Armor During Ballistic Impact, *J. Mater. Des. Appl.*, 2008, **222**, p 259–276
14. M. Grujicic, W.C. Bell, T. He, and B.A. Cheeseman, Development and Verification of a Meso-Scale Based Dynamic Material Model for Plain-Woven Single-Ply Ballistic Fabric, *J. Mater. Sci.*, 2008, **43**, p 6301–6323
15. M. Grujicic, W.C. Bell, G. Arakere, T. He, and B.A. Cheeseman, A Meso-Scale Unit-Cell Based Material Model for the Single-Ply Flexible-Fabric Armor, *Mater. Des.*, 2009, **30**, p 3690–3704
16. M. Grujicic, W.C. Bell, G. Arakere, T. He, X. Xie, and B.A. Cheeseman, Development of a Meso-Scale Material Model for Ballistic Fabric and its Use in Flexible-Armor Protection Systems, *J. Mater. Eng. Perform.*, 2010, **19**(1), p 22–39
17. J.R. Vinson and J.A. Zukas, On the Ballistic Impact of Textile Body Armor, *Trans. ASME J. Appl. Mech.*, 1975, **42**, p 263–268
18. W.A. Taylor, Jr., and J.A. Vinson, Modelling Ballistic Impact into Flexible Materials, *AIAA J.*, 1990, **28**, p 2098–2103
19. S.L. Phoenix and P.K. Porwal, A New Membrane Model for the Ballistic Impact Response and V50 Performance of Multi-Ply Fibrous Systems, *Int. J. Solids Struct.*, 2003, **40**, p 6723–6765
20. J.W. Simons, D.C. Erlish, and D.A. Shockey, Finite Element Design Model for Ballistic Response of Woven Fabrics, *Proceedings of 19th International Symposium on Ballistics*, Interlaken, Switzerland, 2001, p 1415–1422
21. J.M. Walker, Constitutive Model for Fabrics with Explicit Static Solution and Ballistic Limit, *Proceedings of the 18th International Symposium on Ballistics*, San Antonio, TX, 1999, p 1231–1238
22. C.T. Lim, V.P.W. Shim, and Y.H. Ng, Finite Element Modeling of the Ballistic Impact of Fabric Armor, *Int. J. Impact Eng.*, 2003, **28**, p 13–31
23. B.J. Briscoe and F. Motamedi, The Ballistic Impact Characteristics of Aramid Fabrics—The Influence of Interface Friction, *Wear*, 1998, **158**, p 229–247
24. A. Bhatnagar, Bullets, Fragments and Bullet Deformation, *Lightweight Ballistic Composites*, A. Bhatnagar, Ed., CRC Press, New York, 2006, p 29–71
25. S. Kawabata, M. Niwa, and H. Kawai, The Finite-Deformation Theory of Plain-Weave Fabrics Part I: The Biaxial-Deformation Theory, *J. Text. Inst.*, 1973, **64**, p 21–46
26. S. Kawabata, M. Niwa, and H. Kawai, The Finite-deformation Theory of Plain-Weave Fabrics Part II: The Uniaxial-Deformation Theory, *J. Text. Inst.*, 1973, **64**, p 47–61
27. S. Kawabata, M. Niwa, and H. Kawai, The Finite-Deformation Theory of Plain-Weave Fabrics Part I: The Shear-Deformation Theory, *J. Text. Inst.*, 1973, **64**, p 62–85
28. I. Ivanov and A. Tabiei, Loosely Woven Fabric Model with Viscoelastic Crimped Fibres for Ballistic Impact Simulations, *Int. J. Numer. Methods Eng.*, 2004, **61**, p 1565–1583
29. M.J. King, P. Jearanaisilawong, and S. Socrate, A Continuum Constitutive Model for the Mechanical Behavior of Woven Fabrics, *Int. J. Solids Struct.*, 2005, **42**, p 3867–3896
30. P. Boisse, B. Zouari, and A. Gasser, A Mesoscopic Approach for the Simulation of Woven Fiber Composite Forming, *Compos. Sci. Technol.*, 2005, **65**, p 429–436
31. X. Peng and J. Cao, A Dual Homogenization and Finite Element Approach for Material Characterization of Textile Composites, *Composites B Eng.*, 2002, **33**, p 45–56
32. A. Shahkarami and R. Vaziri, A Continuum Shell Finite Element Model for Impact Simulation of Woven Fabrics, *Int. J. Impact Eng.*, 2007, **34**, p 104–119
33. D. Roylance, P. Hammas, J. Ting, H. Chi, and B. Scott, Numerical Modeling of Fabric Impact, in High Strain-Rate Effects on Polymer, Metal and Ceramic Matrix Composites and other Advanced Materials, *Proceedings of the ASME International Mechanical Engineering Congress and Exposition*, Vol 48, San Francisco, 1995, p 155–160
34. P.M. Cunniff, An Analysis of the System Effects in Woven Fabrics Under Ballistic Impact, *Text. Res. J.*, 1992, **62**, p 495–509
35. D. Roylance and S.S. Wang, Influence of Fiber Material Properties on Ballistic Penetration of Textile Panels, *Fiber Sci. Technol.*, 1981, **14**, p 183–190
36. J. Ting, D. Roylance, H. Chi, and B. Chitrangad, Numerical Modeling of Fabric Panel Response to Ballistic Impact, *SAMPE Proceedings*, Philadelphia, PA, 1993, p 384–392
37. V.P.W. Shim, V.B.C. Tan, and T.E. Tay, Modeling Deformation and Damage Characteristics of Woven Fabric Under Small Projectile Impact, *Int. J. Impact Eng.*, 1995, **16**, p 585–605
38. C. Ting, J. Ting, P. Cunniff, and D. Roylance, Numerical Characterization of the Effects of Transverse Yarn Interaction on Textile Ballistic Response, *30th International SAMPE Technical Conference*, October 20-24, 1998, p 57–67
39. D.A. Shockey, J.H. Giovanola, J.W. Simons, D.C. Erlich, R.W. Kolpp, and S.R. Skaggs, *Advanced Armor Technology: Application Potential for Engine Fragment Barrier for Commercial Aircraft*, U.S. Department of Transport, Federal Aviation Administration Report, DOT/FAA/AR97-53, 1997
40. Y. Duan, M. Keefe, T.A. Bogetti, and B.A. Cheeseman, Modeling Friction Effects on the Ballistic Impact Behavior of Single-Ply High-Strength Fabric, *Int. J. Impact Eng.*, 2005, **31**, p 996–1012
41. Y. Duan, M. Keefe, T.A. Bogetti, B.A. Cheeseman, and B. Powers, A Numerical Investigation of the Investigation of the Influence of Friction on Energy Absorption by High-strength Fabric Subjected to Ballistic Impact, *Int. J. Impact Eng.*, 2006, **32**, p 1299–1312
42. B. Gu, Ballistic Penetration of Conically Cylindrical Steel Projectiles into Plain Woven Fabric Target—A Finite Element Simulation, *J. Compos. Mater.*, 2004, **38**, p 2049–2074
43. B.R. Scott and C.F. Yen, Analytic Design Trends in Fabric Armor, *Proceedings of the 22nd International Ballistics Symposium*, 2005, p 752–760
44. M. Boljen and S. Hiermaier, Modeling of Woven Fabrics Used as Lightweight Armor with Respect to Varying Weave Styles and Interplay Friction, *US-German Land Combat Lethality and Survivability Workshop*, 2006
45. T.I. Zohdi and D. Powell, Multiscale Construction and Large-Scale Simulation of Structural Fabric Undergoing Ballistic Impact, *Comput. Methods Appl. Mech. Eng.*, 2006, **195**, p 94–109
46. M.W. Chen and T. Weerasooriya, Experimental Investigation of the Transverse Mechanical Properties of a Singular Kevlar KM2 Fibers, *Int. J. Solids Struct.*, 2004, **41**, p 6215–6232
47. M.W. Chen and T. Weerasooriya, Mechanical Properties of Kevlar KM2 Single Fiber, *J. Eng. Mater. Technol.*, 2005, **127**, p 197–203
48. G. Nilakantan, M. Keefe, J.W. Gillespie Jr., and T.A. Bogetti, Modeling the Material and Failure Response of Continuous Filament Fabrics for Use in Impact Applications, *TexComp 9—International Conference on Textile Composites*, DEStech Publications, Newark, DE, 2008, p 205–214
49. ABAQUS Version 6.10, User Documentation, Dassault Systems, 2010